

Special
Issue

Magnetically Assembled SERS Substrates Composed of Iron–Silver Nanoparticles Obtained by Laser Ablation in Liquid**

Stefano Scaramuzza,^[a] Denis Badocco,^[a] Paolo Pastore,^[a] Diego F. Coral,^[b] Marcela B. Fernández van Raap,^[b] and Vincenzo Amendola^{*[a]}

The widespread application of surface-enhanced Raman scattering (SERS) would benefit from simple and scalable self-assembly procedures for the realization of plasmonic arrays with a high density of electromagnetic hot-spots. To this aim, the exploitation of iron-doped silver nanoparticles (NPs) synthesized by laser ablation of a bulk bimetallic iron–silver target immersed in ethanol is described. The use of laser ablation in liquid is key to achieving bimetallic NPs in one step with a clean surface available for functionalization with the desired thiolated molecules. These iron–silver NPs show SERS performances, a ready response to external magnetic fields and complete flexibility in surface coating. All these characteristics were

used for the magnetic assembly of plasmonic arrays which served as SERS substrates for the identification of molecules of analytical interest. The magnetic assembly of NPs allowed a 28-fold increase in the SERS signal of analytes compared to not-assembled NPs. The versatility of substrate preparation and the SERS performances were investigated as a function of NPs surface coating among different thiolated ligands. These results show a simple procedure to obtain magnetically assembled regenerable plasmonic arrays for repeated SERS investigation of different samples, and it can be of inspiration for the realization of other self-assembled and reconfigurable magnetic–plasmonic devices.

1. Introduction

Surface-enhanced Raman scattering (SERS) offers enormous opportunities for the detection of Raman-active molecules, as demonstrated by the increasing number of analytical and spectroscopic studies involving this technique.^[1–4] Important advantages of SERS are easy sample preparation (often requiring just mixing), the wide gamut of analytes that can be traced (some examples are DNA bases, explosives, drugs, and glucose), and the ultralarge sensitivity (capable, in the best cases, of single-molecule spectroscopy and live-cell imaging).^[1–4]


The SERS effect arises from strong electromagnetic field amplification generated in the proximity of nanostructures.^[1,5] Also, charge-transfer processes between the substrate and analyte can contribute to SERS, if these transitions are in resonance with the excitation wavelength.^[1,2,4] Usually, noble-metal nanostructures, such as patterned surfaces^[2,4,6–9] or nanoparticles (NPs),^[2–4,6,10–12] are used as SERS substrates, although Raman enhancement has also been observed in layers of semi-

conductor and oxide NPs.^[13] In noble metals, the SERS effect is prevalently due to plasmon enhancement of the electromagnetic field at nanometer distances from their surface.^[1,5] In this way, acting much like a nanoantenna, noble-metal nanostructures can boost, by orders of magnitude (up to 10^8 – 10^{12} times), the Raman scattering cross section per molecule, which is usually very small (10^{-30} – 10^{-25} cm²).^[1,2,5] As a substrate for SERS, silver nanostructures show the largest enhancement factors, due to a superior combination of plasmon properties and chemical physical stability relative to other metals, such as gold or aluminum.^[1,6,14,15] On the other hand, transition metals, such as iron, are of limited interest for SERS,^[14–18] due to the absence of plasmon resonance in the visible region and instability in air, but their magnetic properties find multiple analytical applications, for instance, in the realization of responsive nanotools for the separation of analytes in complex mixtures.^[19–23] Hence, a single nanostructure with the plasmonic response of silver and the magnetic properties of iron is exploitable as a powerful SERS substrate that can be manipulated and controlled by external magnetic fields.^[24,25] For instance, multiple analytes, such as viral biomarkers,^[26,27] dopamine,^[28] melamine,^[29,30] arylthiols,^[31] aromatic pollutants,^[32] toxic molecules,^[33,34] or targeted cells,^[35] have been separated and detected by SERS with magnetic–plasmonic substrates. On the other hand, the application of external magnetic fields can be used to direct the assembly of magnetic–plasmonic NPs into arrays of SERS substrates.^[36] Interestingly, these substrates are achievable in a reproducible and scalable way, allowing the preparation of arrays of variable dimensions (varying the

[a] Dr. S. Scaramuzza, Prof. D. Badocco, Prof. P. Pastore, Prof. V. Amendola
University of Padua, Department of Chemical Sciences
Padua (Italy)
E-mail: vincenzo.amendola@unipd.it

[b] Dr. D. F. Coral, Prof. M. B. Fernández van Raap
Physics Institute of La Plata (IFLP-CONICET), Physics Department
Faculty of Exact Sciences, National University of La Plata
La Plata (Argentina)

[**] SERS = Surface-enhanced Raman scattering

 The ORCID identification number(s) for the author(s) of this article can be found under <http://dx.doi.org/10.1002/cphc.201600651>.

 An invited contribution to a Special Issue on Laser Synthesis of Colloids

number of magnets), and that can be cleaned and deposited again.^[3,37] In recent years, this approach was applied to detection systems with the help of microfluidics,^[38] or to the creation of substrates for the detection of analytes such as aromatic molecules^[37,39,40] or organic pollutants.^[41–43]

All of these studies concerned hybrid structures composed of magnetic NPs with a noble-metal moiety, such as heterostructures^[27,28,31,35,42] or core–shells,^[26,30,38,40,41,44–50] which require multiphase synthesis. Sometimes these chemically synthesized NPs showed limitations related to colloidal stability and surface functionalization on demand.^[51]

In recent years, laser ablation in liquid (LAL) has emerged as a reliable approach for the preparation of magnetic and plasmonic NPs in one step, even with unconventional structures or thermodynamically inhibited compositions.^[52] Nanostructures with magnetic and plasmonic responses obtained so far by this method include gold–iron^[14,18,53,54] and silver–iron nanoalloys,^[25] nanocrescents,^[54] and core–shell structures with either a plasmonic core and magnetic oxide shell^[54] or a magnetic iron core and plasmonic shell.^[55] Similarly, interesting nanosystems were also obtained by laser irradiation of a mixture of NPs, such as solid solutions of gold and nickel,^[56,57] iron,^[58] or cobalt.^[59]

Herein, to achieve a versatile nanomaterial endowed with magnetic and plasmonic properties, easy surface chemistry, and complete colloidal stability, as required for the realization of magnetically assembled and reusable SERS substrates, we synthesized iron-doped silver NPs by LAL. By this approach, NPs with magnetic and plasmonic properties are obtained in one step, and the particle surface remains available for functionalization with the desired thiolated ligands. We tested the effect of different types of ligands anchored to the surface of NPs for magnetic assembly into SERS substrates and relative SERS performances. After selection of the best surface coating, regeneration of the SERS substrate for the detection of typical analytes, such as fungicides or pesticides, was successfully assessed. Overall, we show a simple way to obtain magnetically assembled arrays of plasmonic NPs for use as regenerable SERS substrates, which can be of inspiration for the realization of other self-assembled and reconfigurable magnetic–plasmonic arrays.

Experimental Section

The LAL of Fe-doped Ag NPs was performed by focusing $\lambda = 1064$ nm (6 ns, 50 Hz, 120 mJ/pulse) laser pulses with a 15 cm focal lens on a bimetallic target (66% atomic Ag – 34% atomic Fe, from MaTeck GmbH) dipped in ethanol (HPLC grade, from Sigma–Aldrich), with a fluence of 7 J cm^{-2} . After the synthesis, thiolated ligands were added to the Fe–Ag NP colloids and sonicated for 20 min. The following ligands were used for surface functionalization of Fe–Ag NPs: 2-mercaptoethanol (ME; 78.13 Da, from Fluka), sodium-3-mercapto-1-propanesulfonate (MPS; 178.21 Da, from Sigma–Aldrich), glutathione (GSH; 307.32 Da, from Sigma–Aldrich), *O*-(2-mercaptoethyl)-*O'*-methylhexa(ethylene glycol) (PEG350; 356.48 Da from Sigma–Aldrich), and poly(ethylene glycol) methyl ether thiol (PEG800; 800 Da average molecular weight, from Sigma–Aldrich). These ligands were selected for the absence of

background Raman signals under our experimental conditions. Thiols were added at a final concentration of $2 \mu\text{M}$ to a 0.1 mg mL^{-1} solution of Fe–Ag NPs in ethanol ($10 \mu\text{L}$ of added ligand solution per mL of Fe–Ag NP solution, corresponding to ≈ 500 ligands per Fe–Ag NP). The solution was then reduced in volume by using a rotating evaporator, diluted 1:1 with demineralized water, and treated with a 2 mg mL^{-1} aqueous solution of ethylenediaminetetraacetic acid disodium salt dehydrate (EDTA; from Sigma–Aldrich) at 30°C for 1 h. This temperature was selected because surface oxidation of silver NPs in an aqueous environment could occur at higher temperatures, with subsequent release of Ag^+ ions.^[60] Then, the solutions were purified by at least four dialysis runs with Sartorius Vivaspin concentration membranes (cutoff: 10000 Da), and finally the NPs were resuspended in demineralized water. EDTA and dialysis were required to remove byproducts of the synthetic process, such as amorphous iron oxides and hydroxides, according to a previously reported procedure.^[14,18,53]

Ag NPs were obtained by using the same LAL procedure and parameters, with a silver (99.99%) bulk target dipped in ethanol solution.

Plasmonic substrates were obtained by pouring the colloid on a soda lime glass slide placed on top of an array of NdFeB cylindrical magnets (4 mm in diameter per 8 mm of length). The poles of the magnets (located on the cylinder faces) were oriented towards the surface of the slide, and magnets were packed with the highest density corresponding to a distance of 4 mm between their axes. The volume of the colloid was set to have $20 \mu\text{L}$ of a 4 mg mL^{-1} dispersion of NPs ($80 \mu\text{g}$ of NPs) for each magnet. After deposition, the solution was left to dry at 20°C for overnight (16 h).

For the SERS experiments, we used 4-[[4-(dimethylamino)phenyl]-(phenyl)methylidene]-*N,N*-dimethylcyclohexa-2,5-dien-1-iminium chloride (MG, also called malachite green; from Sigma–Aldrich) and sodium (diethylcarbamothioyl)sulfanide (DTC; from Sigma–Aldrich). All analytes were dissolved in water, and $5 \mu\text{L}$ of the solution (10 pmol) was drop-casted on the SERS spot prior to analysis. In the case of 2D Raman maps, the analytes were mixed with the Fe–Ag NP colloids before deposition. All spectra were subjected to baseline subtraction with the built-in Renishaw WiRe 3.4 spline cubic interpolation routine.

Regeneration of SERS substrates was performed in three steps by 1) redispersing the NPs in a 10^{-4} M aqueous solution of NaCl (1 mL) by bath ultrasonication for 30 min with a Branson CPXH sonicator; 2) washing twice with distilled water by centrifugation for 10 min at 15000 rcf with an Eppendorf centrifuge model 5430 equipped with a fixed-angle rotor model FA-45-24-11-HS; and 3) bringing the colloid to the pristine NP concentration and repeating the magnetic assembly of the plasmonic substrate, according to the above-mentioned array-formation procedure.

Optical absorption spectroscopy was performed with a Varian Cary 5 UV/Vis spectrometer by using 2 mm optical path quartz cells. TEM was performed with a FEI Tecnai G2 12 instrument operating at 100 kV and equipped with a TVIPS charge-coupled device (CCD) camera. EDS analysis was performed at 300 kV with a JEOL JEM 3010 microscope by using a Gatan Multiscan CCD 794 camera and an EDS spectrometer (Oxford Instruments). Fe–Ag NPs were deposited by drop-casting on a carbon-coated copper grid.

Dynamic light scattering (DLS) and Z spectroscopy was performed with a Malvern Zetasizer Nano ZS in DTS1070 cells.

Metal concentrations were determined by inductively coupled plasma mass spectrometry (ICP-MS) performed with an Agilent Technologies 7700x ICP-MS instrument (Agilent Technologies International Japan, Ltd., Tokyo, Japan). The instrument was equipped with an octopole collision cell operating in kinetic energy discrimination mode, which was used for the removal of polyatomic and argon-based interferences. The operating conditions and data acquisition parameters were reported elsewhere.^[61] The multielement calibration standard-3 (Agilent Technologies) for Ag and CLPP-CAL-1 (Inorganic Ventures' Calibration Standard 1) for Fe were used. Multielement standard solutions for calibration were prepared in 5% aqua regia by gravimetric serial dilution at six different concentrations (from 0.5 to 1000 $\mu\text{g L}^{-1}$). The non-parametric Theil regression was used.^[62] A microwave acidic digestion was performed with a CEM EXPLORER SP-D PLUS instrument. NPs were digested in aqua regia according to the following microwave acid mineralization procedure: ramp temperature from room temperature to 200 °C in 5 min, then 200 °C for 15 min; pressure 400 psi and power 300 W.

Magnetic characterization was performed by using a Quantum Design superconducting quantum interference device (SQUID) operated at a maximum field of $\mu_0 H_{\text{max}} = 2.5$ tesla. Specific magnetization (M) as a function of applied magnetic field (H) was obtained at 5 and 300 K, and magnetization temperature dependences under zero-field-cooled (ZFC), field-cooled (FC), and thermoremanent magnetization (TRM) protocols were measured at 5 K min^{-1} by using a dc field of 4 kA m^{-1} (50 Oe). Measurements were performed on liquid or frozen colloids, depending on the measurement temperature. The colloidal suspension (50 μL) at a concentration of 0.29 $\text{mg}_{\text{Fe}} \text{mL}^{-1}$ were sealed into a heat-shrinkable tube to prevent sample evaporation and spillage. Data were shown after subtracting the diamagnetic contribution due to solvent and Ag.

Raman spectroscopy was performed with a Renishaw InVia micro-Raman spectrometer equipped with a Leica 5X microscope objective, a motorized piezo stage controlled by the WiRe 4 software, and a He-Ne $\lambda = 633$ nm laser line with 0.3 mW of excitation power and acquisition times of 30 s for each analysis.

2. Results

The iron-doped silver NPs obtained by the LAL procedure described in Figure 1A have an average size of (15 ± 5) nm, as observed by TEM (Figure 1B), and they appear to be composed of a mixture of small NPs with spherical shapes and some large "truffle-like" nanostructures, in agreement with a previous report.^[25] To obtain more insights into the formation of Fe-Ag NPs, we followed an early report by Mafunè et al.,^[63] who suggested that NP formation included a stage of coalescence of smaller nuclei. This was inferred from the experimental observation that the size of the NPs was much lower when the liquid contained an appreciable amount of ligands that could bind and stabilize the surface of NPs, while maintaining all other synthetic parameters the same.^[63,64] Therefore, we performed a similar experiment to compare the size and morphology of Fe-Ag NPs obtained in the absence and in the presence of ligands capable of strong binding to the surface of the particles, while maintaining all other experimental parameters the same. For this experiment, we selected the thiolated ligand PEG350, dissolved at a concentration of 2 mg mL^{-1} in ethanol, before or after LAL. TEM images clearly show that Fe-Ag NPs are grouped into small agglomerates and are surrounded by an amorphous matrix typically ascribable to iron

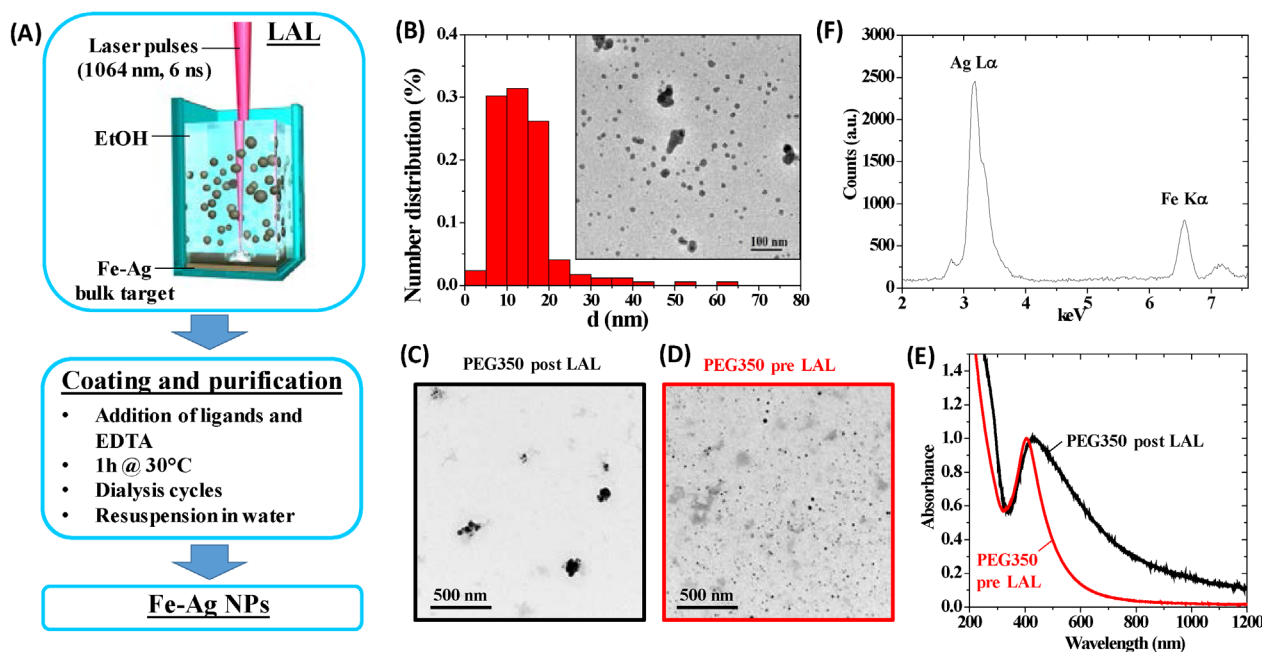


Figure 1. A) Sketch of Fe-Ag NP preparation: NPs are obtained by LAL in ethanol, then mixed with thiols and EDTA, and finally cleaned by dialysis. B) Representative TEM image and size distribution of Fe-Ag NPs. C) TEM image of Fe-Ag NPs obtained after LAL followed by the addition of PEG350. D) TEM image of Fe-Ag NPs obtained after LAL in a solution of PEG350 added before the synthesis. E) UV-Vis absorption spectra of the solution of Fe-Ag NPs obtained by LAL with PEG350 added after (black line) or before (red line) the synthesis. F) EDS spectrum collected on a Fe-Ag NPs deposit, showing the Ag $L\alpha$ and Fe $K\alpha$ peaks.

oxide byproducts (Figure 1C). This matrix is efficiently dissolved during the purification procedure with EDTA and dialysis, as appreciable by comparison of Fe–Ag NPs in Figure 1B (after purification) and C (just after the synthesis and addition of PEG350), releasing the final mixture of small NPs with spherical shapes and some large truffle-like nanostructures. Conversely, the addition of PEG350 before LAL dramatically changes the average size and morphology of Fe–Ag NPs, with a drastic reduction in the size of the NPs and aggregation, as well as almost complete disappearance of the truffle-like nanostructures (Figure 1D). This is further corroborated by UV/Vis spectroscopy: the surface plasmon band maximum at $\lambda \approx 420$ nm is much broader in case of the agglomerated Fe–Ag NPs for which PEG350 is added after LAL (black line in Figure 1E), than in the sample for which PEG350 is added before LAL (red line in Figure 1E). According to these findings, we definitively concluded that the formation of FeAg NPs involved a stage of nuclei coalescence, as proposed by Mafunè et al.,^[63] and we could exclude the possibility that truffle-like nanostructures were directly formed by ejection of liquid droplets from the solid target during laser ablation.

The composition of Fe–Ag NPs was qualitatively assessed by EDS analysis performed on the purified and dried sample deposited on a soda lime glass by drop-casting, and evidenced by the presence of both Ag $L\alpha$ (3.0 keV) and Fe $K\alpha$ (6.4 keV) peaks (Figure 1F). This is in agreement with the line scan EDX mapping results performed on individual Fe–Ag NPs agglomerates reported in our previous study.^[25] In particular, in the same study, we showed by various investigation techniques that Fe–Ag NPs were composed of ordered Ag crystalline domains alternated with disordered Fe–Ag regions that were randomly distributed inside the volume of each NP.^[25]

Quantitatively, the composition of the Fe–Ag NPs was assessed by ICP-MS, resulting in (80 ± 6) at% Ag and (20 ± 5) at% Fe. The composition of Fe–Ag NPs deviates from that of the bulk target, which means that a fraction of Fe is lost during the synthesis. Therefore, we analyzed the elemental composition of synthetic products in the main stages of the synthetic

procedure, and we found that just after the synthesis there was (40 ± 8) at% Fe and (60 ± 10) at% Ag. This ratio is comparable to the target composition within experimental error. After the purification stage, this composition changes to a final value of 20 at%/80 at% Fe/Ag, and the dialyzed waste solution contains (83 ± 8) at% Fe and (17 ± 3) at% Ag. Interestingly, we found that (52 ± 7)% of the total ablated mass was lost during the purification procedure; part of it was dissolved during heat treatment to form molecular compounds or small NPs with sizes below the cutoff of the dialysis membrane [(24 ± 5)% of the total ablated mass], and part was irreversibly attached to the dialysis membrane after centrifugation [(28 ± 5)% of the total ablated mass].

The magnetic properties of the Fe–Ag NPs were investigated by dc magnetometry, which showed that $M(H)$ has a typical superparamagnetic behavior. This means that Fe–Ag NPs are single magnetic domains. At 300 K, the hysteresis loop was well fitted with two Langevin functions, which indicated two characteristic sizes of (2.0 ± 1.6) (52% of the particles) and (7.1 ± 0.3) nm (48%), plus a small linear (positive slope) contribution known as high-field susceptibility (Figure 2A). The observation of two different populations of magnetic NPs is in agreement with the polycrystalline and highly defective nature of these bimetallic particles obtained by LAL. We previously reported the alternation of large metal Ag domains and small disordered Fe–Ag ones.^[25] At room temperature, we measured a fitted saturation magnetization of (81 ± 2) Am²kg_{Fe}⁻¹ (Figure 2A). At 5 K, the magnetization curve shows a hysteresis with a coercive field of $H_c = (434 \pm 10)$ Oe (Figure 2B), and saturation magnetization is not reached within the experiment. This is ascribable to high-field susceptibility related to surface magnetic disorder induced by the lack of symmetry.^[65] However, saturation magnetization derived from the fit is (87 ± 39) Am²kg_{Fe}⁻¹. ZFC/FC/TRM measurements (Figure 2B) are consistent with a distribution of energy barriers for magnetization reversal, and suggest that the blocking temperature of Fe–Ag NPs is moderately greater than room temperature. ZFC data were well fitted with the model reported by Tournus and

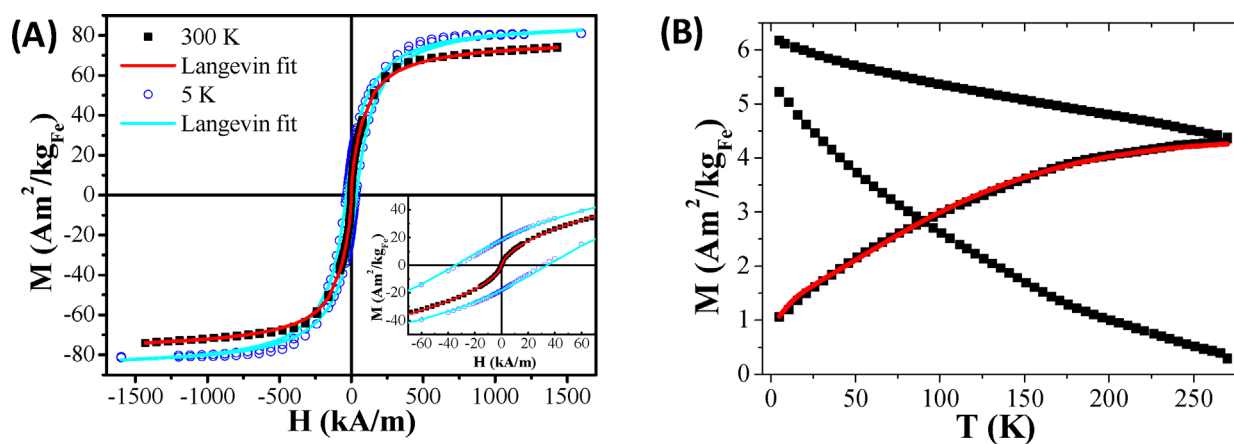


Figure 2. A) Hysteresis loops collected at 300 K (black squares) and 5 K (blue circles), and relative Langevin fits (red and cyan lines for 300 K and 5 K, respectively). B) Temperature dependence of ZFC/FC/TRM magnetization measured with a 4 kA m⁻¹ probe field (black squares) and fitted with a Tournus model (red line).

Bonet,^[66] by considering the two characteristic sizes derived from M(H) analysis, and we obtained an extrapolated mean blocking temperature of 319 K.

The coating of Fe–Ag NPs with thiolated ligands is necessary to prevent irreversible sedimentation of the colloidal system in aqueous solution and in organic solvents, as required for magnetic assembly and reusability of the plasmonic substrate. To this aim, we tested five types of thiolated molecules: three neutral ligands with increasing chain length (ME, PEG350, and PEG800) and two anionic ligands (GSH and MPS). By UV/Vis absorption spectroscopy, a sharp plasmon band maximum at $\lambda \approx 420$ nm is observed in the aqueous dispersions of NPs coated with MPS, PEG350, or PEG800 (Figure 3 A); this can be used to assess the satisfactory colloidal stability of the three samples. The absorption band of Fe–Ag NPs coated with GSH is redshifted to $\lambda \approx 500$ nm (blue line in Figure 3 A), which suggests that extensive particle aggregation occurs with this ligand. ME caused the dissolution of NPs, forming an opalescent Ag–thiol layered compound, as demonstrated by the characteristic absorption band at a wavelength shorter than $\lambda = 390$ nm (magenta line in Figure 3 A).^[67–69]

The magnetic response of the ligand-coated Fe–Ag NPs was easily probed by placing some drops of each colloid on a soda lime glass lying on top of an array of NdFeB magnets; this assisted the collection of NPs in millimeter-sized spots corresponding to the positions of the magnets after overnight incubation and evaporation of the liquid (Figure 3 B). Although NPs in MPS, PEG350, PEG800, and GSH samples all responded to the magnetic field and accumulated in concomitance to the magnets, the sharpest deposits are observed for the MPS and the PEG800 samples; this is indicative of the superior colloidal stability of these NPs and subsequent superior ability to accumulate in the region with the largest magnetic field on the timescale of the experiment. Due to NP degradation in pres-

ence of ME, no response to the magnetic field was observed for the ME sample, which was not considered further. The NPs in PEG350 and GSH samples are spread over a wider area, which suggests that sedimentation competes with magnetic assembly. In the case of GSH coating, one can also note that carboxylic groups may have stronger affinity to the glass surface than the other ligands,^[70,71] accelerating the sticking of NPs on the substrate before migration to the area with greater intensity of magnetic field can occur. However, DLS and z-spectroscopy measurements suggest that a more rapid sedimentation of GSH-coated NPs is the main reason for their lower ability to accumulate in concomitance to magnets; these particles have lower z potential and a much larger hydrodynamic size $[(-22 \pm 13)$ mV and (1005 ± 577) nm] than those of MPS-coated NPs $[(-47 \pm 13)$ mV and (78 ± 34) nm]. In particular, MPS-coated NPs have a lower hydrodynamic size and larger z-potential than NPs obtained after LAL or after the addition of EDTA (see Table 1). It is worth noting that solution pH was not regulated by the addition of saline buffers, and resulted in pH = 5.0 in both the solutions of GSH and MPS. Therefore, the addition of a pH buffer may change the parameters for colloidal stability, although at the price of adding salt residuals during sample drying on the glass substrate.

The SERS performances of the four plasmonic arrays were tested by monitoring the intensity of the $\tilde{\nu} = 1617$ cm^{-1} band of MG in the plasmonic spots, and we found that the MPS provided the best signals (Figure 3 C). One possible explanation is that MPS has the lowest molecular weight among the four; thus allowing the lowest distance between analytes and particles surface in the magnetically assembled NPs spot, and analyte diffusion into NPs interstices is facilitated when the surface of the particles is coated with short-chain ligands. This is relevant for the SERS performances because the largest electromagnetic field enhancements are observed at interstices and

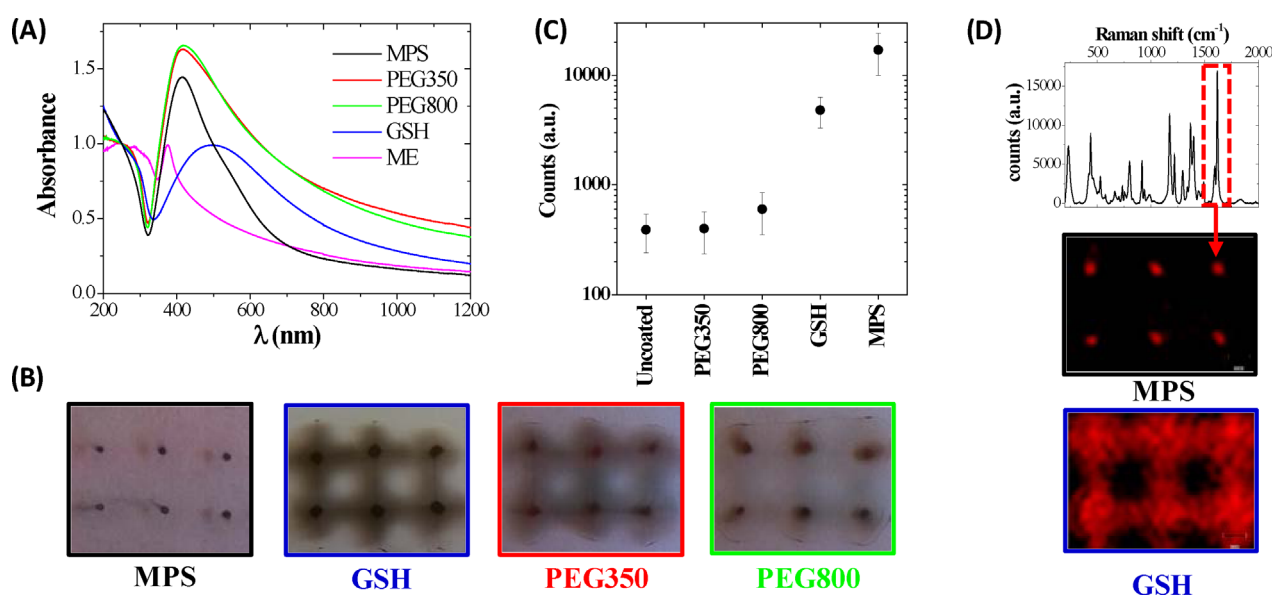


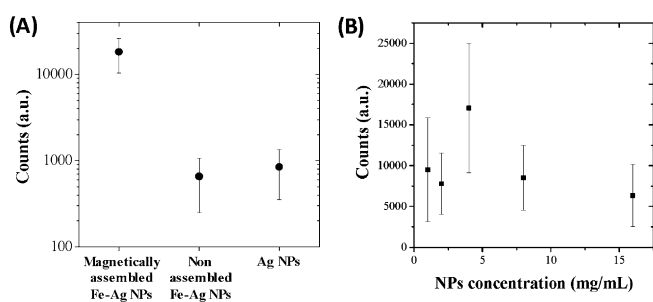
Figure 3. A) UV/Vis absorption spectra of Fe–Ag NPs coated with different ligands. B) Photographs of magnetically assembled Fe–Ag NPs on soda lime glass. The distance between spots is 4 mm. C) Intensity of the MG Raman band at $\tilde{\nu} = 1617$ cm^{-1} measured on Fe–Ag NPs with different surface coatings. D) 2D Raman map of the $\tilde{\nu} = 1617$ cm^{-1} band of MG collected on the two best performing substrates (Fe–Ag NPs coated with MPS or GSH).

Table 1. Hydrodynamic size, z potential, and pH of Fe–Ag NPs with various coatings at different stages of the synthetic procedure. The liquid environment is indicated for each sample.

Sample	Liquid	DLS size [nm]	z potential [mV]	pH
Fe–Ag NPs after LAL	ethanol/water 1:1 (diluted 1:1 in water after LAL)	307 ± 145	−27 ± 5	6.5 ± 0.5
Fe–Ag NPs after addition of EDTA	ethanol/water 1:1	241 ± 132	−14 ± 8	4.0 ± 0.5
MPS-coated Fe–Ag NPs	water	78 ± 34	−47 ± 13	5.0 ± 0.5
GSH-coated Fe–Ag NPs	water	1005 ± 577	−22 ± 13	5.0 ± 0.5

tight or concave junctions between plasmonic NPs.^[1,4,6,11] As shown in Figure 3C, SERS signals in Fe–Ag NPs obtained from LAL are the lowest. This is clearly explained by the presence of iron byproducts embedded in the plasmonic NPs before treatment with EDTA and the washing procedure (see, for instance, Figure 1C). Additionally, magnetic assembly is poor due to the rapid sedimentation of these NPs, which show a lower z potential and larger hydrodynamic size than those of MPS-coated Fe–Ag NPs (see Table 1). It is worth emphasizing that the same experiment cannot be performed on Fe–Ag NPs treated with EDTA and dialyzed without the addition of stabilizing ligands because, in this case, there is no recovery of NPs after dialysis with concentration membranes, due to 100% NP adsorption on the dialysis membrane.

Additional evidence about the best performance of the MPS sample is obtained when looking at the bidimensional Raman map of the $\tilde{\nu} = 1617 \text{ cm}^{-1}$ band of MG (Figure 3D). In the array obtained from the MPS sample, the SERS signal is well localized on the plasmonic spot, whereas in the GSH sample the Raman signal is spread over a large area and the average signal intensity in the plasmonic spots is three times lower. This finding suggests that localization of NPs in a small area by magnetophoresis is beneficial for the SERS signal, and we obtained further direct evidence of it by measuring the SERS signal on the MPS sample with and without magnetic assem-

**Figure 4.** A) Average intensity of the MG Raman band at $\tilde{\nu} = 1617 \text{ cm}^{-1}$ in different SERS substrates: magnetically assembled Fe–Ag NPs, Fe–Ag NPs deposited without external magnetic field for assembly, and Ag NPs. In all cases, NPs were coated with MPS. B) Average intensity of the MG Raman band at $\tilde{\nu} = 1617 \text{ cm}^{-1}$ in SERS substrates of magnetically assembled Fe–Ag NPs deposited from a colloidal solution with concentrations varying from 16 to 1 mg mL⁻¹. Each point is obtained from the average of at least six magnetically assembled spots.

bly, by keeping all other experimental parameters the same (Figure 4A). A 28-fold difference in the Raman scattering intensity is observed in magnetically focused substrates, although the plasmonic nanomaterial is the same in both cases. Additionally, we compared the SERS performances with MPS-coated pure Ag NPs obtained by the same LAL procedure and brought to the same silver concentration of the other spotted solution. Because Ag NPs do not respond to the applied magnetic field, that is, no assembly in a localized area is possible, the SERS signal is much lower than that of the magnetically assembled Fe–Ag NPs, although it is comparable to that of Fe–Ag NPs without application of the

magnet. It is worth noting that, in this experiment, the solution of analyte was spotted on the already formed plasmonic substrates, with or without magnetic assembly; thus providing the analyte under the same conditions independent of the magnetophoretic collection of NPs. This definitively substantiated the role played by the localization of metal nanostructures in a confined area, rather than spread over the glass slide after liquid evaporation. It is worth stressing that, without magnetic focusing, about 15 times more material would be necessary to obtain the same concentration of NPs over the whole spotted area as that reached in the magnetically assembled plasmonic spot.

We further explored the dependence of the SERS response on the amount of plasmonic NPs accumulated in the spot, by monitoring the intensity of the $\tilde{\nu} = 1617 \text{ cm}^{-1}$ MG peak as a function of the concentration of NPs in the solution exploited for magnetic assembly, while maintaining the same volume of liquid spotted on the glass slide during the process. The results reported in Figure 4B show little dependence on the concentration of NPs, although an optimum concentration of 4 mg mL⁻¹ is found. The decrease in the SERS signal for concentrations lower than 4 mg mL⁻¹ can be ascribed to the lower amount of plasmonic NPs in the magnetically assembled spots, and is in agreement with the same trend observed in Figure 4A for non-assembled Fe–Ag NPs or pure Ag NPs, for which the same amount of plasmonic NPs was spread over a larger surface than that of the magnetically assembled spot. Instead, the decrease in the SERS intensity at a concentration higher than 4 mg mL⁻¹ may be ascribed to NP self-absorption of the excitation laser beam and Raman scattered radiation, if the optimal thickness of the plasmonic spot is exceeded.

By maintaining the optimal concentration of NPs and volume of colloid per magnet, while increasing linearly the number of magnets exploited for the assembly, we obtained a 5 × 11 array of plasmonic spots (Figure 5A). SERS was detected in all plasmonic spots of the array (Figure 5B), although, in some cases, the spots at the borders of the array generated a less-intense SERS signal. Indeed, a lower amount of material is accumulated in spots along the perimeter due to the drag force of the liquid during its evaporation. Under our experimental conditions, this problem can be prevented by maintaining a distance of the order of 5 mm between the array of mag-

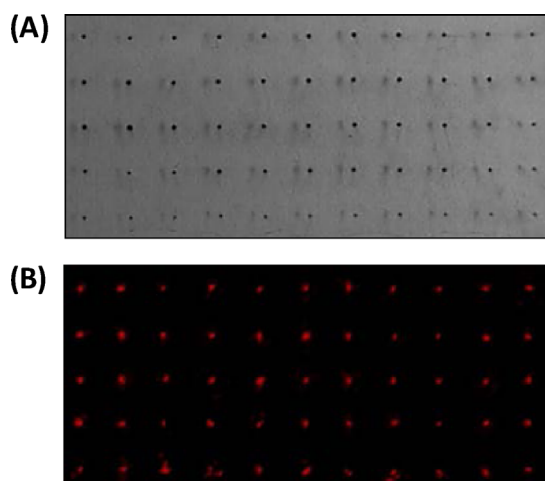


Figure 5. A) Photograph of an array of 5×11 magnetically assembled SERS substrates obtained in one step from a single solution of Fe–Ag NPs deposited on a glass slide. B) 2D map of the $\tilde{\nu} = 1617 \text{ cm}^{-1}$ Raman band of MG collected on the SERS array.

nets and the border of the underlying liquid at the moment of its deposition on the glass slide.

Stabilization of Fe–Ag NPs with a thiolated ligand is key to the reversibility of the magnetic assembly, even after complete drying of the dispersing solvent. We exploited this feature for the regeneration of SERS substrates by redissolving NPs in water, washing the analyte by centrifugation, and repeating the magnetic assembly on a new glass slide. We successfully applied this procedure to the detection, in sequence, of MG, which is an antifungal and antibacterial additive,^[38] and DTC, which is a pollutant pesticide,^[72] by exploiting the same Fe–Ag NPs after regeneration (Figure 6).

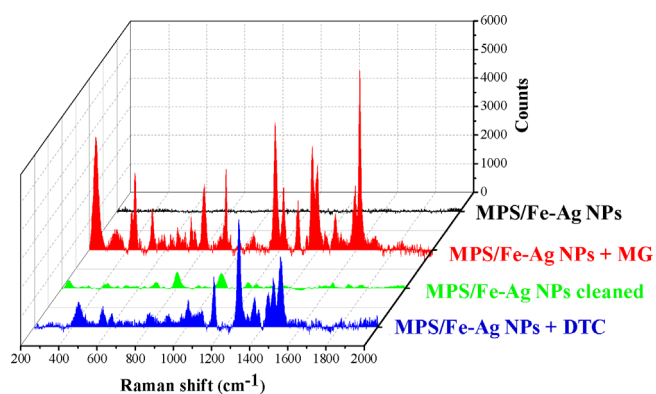


Figure 6. Raman spectra of magnetically assembled MPS-coated Fe–Ag NP substrates before the addition of MG (black line); after the addition of MG (red line); after cleaning of the same Fe–Ag NPs, according to the procedure described in the text (green line); and after the addition of DTC (blue line).

3. Discussion

Using Fe-doped Ag NPs obtained by LAL, the magnetic assembly of plasmonic NPs into an ordered array of SERS substrates was possible. In this way, we observed a 28-fold increment of

the SERS signal collected from the plasmonic spots, relative to the same NPs spotted on the glass slide without magnetic assembly or to a reference of nonmagnetic pure Ag NPs. Therefore, the coexistence of magnetic and plasmonic properties in the same NPs allowed better exploitation of the SERS potentials of these nanomaterials. The increment in SERS signal is due to increased scattering of light in the plasmonic substrate and to a higher concentration of electromagnetic hot spots in the magnetically induced aggregates.^[36,51] However, our experiments showed that light scattering and absorption in the plasmonic spot could be detrimental to SERS analysis, if a critical NP concentration threshold was exceeded in the solution deposited for the magnetic assembly.

The colloidal stability of NPs was crucial to permit the magnetophoretic assembly instead of bare precipitation onto an area extended by more than about 15 times. This means that, without magnetic focusing, the same SERS performances would be obtained by using about 15 times more NPs in the same volume of liquid. The appropriate selection of ligands is important to obtain the best compromise between colloidal stability and short distance between analyte and the surface of the plasmonic NPs, as required for the largest enhancement of the electromagnetic field at interstices and tight or concave junctions between metal particles. Therefore, it is possible that MPS provided the best results among the five ligands tested because of the chemical stability of the MPS–NP system and small molecular structure (178.21 Da). When longer thiols, such as PEG350, were used, no appreciable Raman enhancement was observed, which suggested that such ligands formed a layer impenetrable to analytes that could not reach the tiniest junctions between NPs, where SERS is more efficient. Indeed, according to reports in the literature, about 2 nm is the critical distance required for achieving enhancements of the order of at least 10^4 .^[3,6,37,73] This is larger than the length of two MPS molecules, which is roughly in the order of $2 \times 0.6 \text{ nm} = 1.2 \text{ nm}$.

On the other hand, passivation of Fe–Ag NPs with small thiolated ligands was key to the reversible magnetic assembly of plasmonic spots, which enabled the reusability of the SERS substrates. The need for reusable substrates for SERS analysis appeared recently as a cost-effective strategy for repeated analytical assays.^[3,37] Different approaches to this problem have been used in the past, with promising results, such as electrochemical stripping,^[74] dipping in solutions of concentrated acid,^[75] ultraviolet–ozone (UVO) cleaning,^[76] or metal nanostructures supported on photocatalytic oxides (e.g. TiO_2 or ZnO microspheres).^[77–80] However, photocatalytic SERS substrates initiate the degradation of analytes during sample preparation and Raman measurement, due to light exposure, and this requires the analysis to be performed a short time after sample deposition.^[79] Solutions of concentrated acid may destroy both the analyte and nanostructured noble-metal surface.^[81] UVO cleaning and metal stripping can be performed on demand, but they require a UVO cleaning chamber or complete electrochemistry setup, respectively.^[74] Our method has the advantage of requiring minimal equipment that is easily available in almost every laboratory, such as a benchtop centrifuge, small

magnets, and a ultrasonic bath, while maintaining comparable results in terms of substrate reusability. Additionally, the operator is free to decide the best time to regenerate the substrate.

4. Conclusions

We reported the use of laser-ablated Fe–Ag NPs for the magnetic assembly of plasmonic arrays that could serve as regenerable SERS substrates. To this aim, LAL played a crucial role for achieving, in one step, bimetallic NPs composed of two thermodynamically immiscible metals, such as iron and silver, and with a clean surface available for functionalization with the desired thiolated molecules. The iron-doped silver NPs obtained by LAL showed SERS performances, ready responses to external magnetic fields, and complete flexibility in surface coating. The magnetic assembly of Fe–Ag NPs, performed with a set of small NdFeB magnets, allowed a 28-fold increase of the SERS signal relative to that of non-assembled NPs. The ease of substrate preparation and SERS performances were investigated as a function of NP surface coating for different thiolated ligands, and the best compromise between colloidal stability and small interparticle gaps was observed with MPS. Additionally, due to NP surface stabilization, the SERS arrays could be regenerated after use by a relatively simple procedure, exploiting only an ultrasonic bath and a small benchtop centrifuge. These results can be of inspiration for the realization of other self-assembled and reconfigurable magnetic–plasmonic devices.

Acknowledgements

Prof. M. Meneghetti is gratefully acknowledged for useful discussions and advice. Financial support from the University of Padua (PRAT no. CPDA114097/11 and Progetto Strategico STPD11RYPT 001), Conicet (PIP 0720), and UNLP (X11/680) is gratefully acknowledged.

Keywords: magnetic properties · nanoparticles · Raman spectroscopy · self-assembly · surface chemistry

- [1] M. Moskovits, *Phys. Chem. Chem. Phys.* **2013**, *15*, 5301–5311.
- [2] J. Kneipp, H. Kneipp, K. Kneipp, *Chem. Soc. Rev.* **2008**, *37*, 1052–1060.
- [3] W. Xie, S. Schlücker, *Rep. Prog. Phys.* **2014**, *77*, 116502.
- [4] C. L. Haynes, A. D. McFarland, R. P. V. Duyne, *Anal. Chem.* **2005**, *77*, 338A–346A.
- [5] E. Le Ru, E. Blackie, M. Meyer, P. Etchegoin, *J. Phys. Chem. C* **2007**, *111*, 13794–13803.
- [6] G. McNay, D. Eustace, W. E. Smith, K. Faulds, D. Graham, *Appl. Spectrosc.* **2011**, *65*, 825–837.
- [7] S. M. Tabakman, Z. Chen, H. S. Casalongue, H. Wang, H. Dai, *Small* **2011**, *7*, 499–505.
- [8] A. De Bonis, A. Galasso, N. Ibris, M. Sansone, A. Santagata, R. Teghli, *Surf. Coat. Technol.* **2012**, *207*, 279–285.
- [9] A. Wolosiuk, N. G. Tognalli, E. D. Martínez, M. Granada, M. C. Fuertes, H. Troiani, S. A. Bilmes, A. Fainstein, G. J. Soler-Illia, *ACS Appl. Mater. Interfaces* **2014**, *6*, 5263–5272.
- [10] L. Guerrini, D. Graham, *Chem. Soc. Rev.* **2012**, *41*, 7085–7107.
- [11] V. Amendola, M. Meneghetti, *Adv. Funct. Mater.* **2012**, *22*, 353–360.
- [12] H. Tamamitsu, K. Saitow, *Chem. Phys. Lett.* **2014**, *591*, 37–42.
- [13] X. Tan, J. Melkersson, S. Wu, L. Wang, J. Zhang, *ChemPhysChem* **2016**, *17*, 2630–2639.
- [14] V. Amendola, S. Scaramuzza, S. Agnoli, S. Polizzi, M. Meneghetti, *Nanoscale* **2014**, *6*, 1423–1433.
- [15] M. G. Blaber, M. D. Arnold, M. J. Ford, *J. Phys. Condens. Matter* **2010**, *22*, 143201.
- [16] L. Guo, Q. Huang, X. Li, S. Yang, *Phys. Chem. Chem. Phys.* **2001**, *3*, 1661–1665.
- [17] Z. Tian, Z. Yang, B. Ren, J. Li, Y. Zhang, X. Lin, J. Hu, D. Wu, *Faraday Discuss.* **2006**, *132*, 159–170.
- [18] V. Amendola, S. Scaramuzza, L. Litti, M. Meneghetti, G. Zuccolotto, A. Rosato, E. Nicolato, P. Marzola, G. Fracasso, C. Anselmi, M. Pinto, M. Colombatti, *Small* **2014**, *10*, 2476–2486.
- [19] V. Amendola, M. Meneghetti, G. Granozzi, S. Agnoli, S. Polizzi, P. Riello, A. Boscaini, C. Anselmi, G. Fracasso, M. Colombatti, *J. Mater. Chem.* **2011**, *21*, 3803–3813.
- [20] A. H. Latham, M. E. Williams, *Acc. Chem. Res.* **2008**, *41*, 411–420.
- [21] V. T. Tran, H. Zhou, S. Lee, S. C. Hong, J. Kim, S. Jeong, J. Lee, *ACS Appl. Mater. Interfaces* **2015**, *7*, 8650–8658.
- [22] K. Gmucová, M. Weis, V. Nádaždy, E. Majková, *ChemPhysChem* **2008**, *9*, 1036–1039.
- [23] X. Zhao, N. S. Hosmane, A. Wu, *ChemPhysChem* **2012**, *13*, 4142–4147.
- [24] K. J. Major, C. De, S. O. Obare, *Plasmonics* **2009**, *4*, 61–78.
- [25] V. Amendola, S. Scaramuzza, S. Agnoli, G. Granozzi, M. Meneghetti, G. Campo, V. Bonanni, F. Pineider, C. Sangregorio, P. Ghigna, S. Fiameni, L. Nodari, *Nano Res.* **2015**, *8*, 4007–4023.
- [26] C. Yuen, Q. Liu, *Analyst* **2013**, *138*, 6494–6500.
- [27] J. Neng, M. H. Harpster, W. C. Wilson, P. A. Johnson, *Biosens. Bioelectron.* **2013**, *41*, 316–321.
- [28] V. Ranc, Z. Markova, M. Hajduch, R. Prucek, L. Kvitek, J. Kaslik, K. Safarova, R. Zboril, *Anal. Chem.* **2014**, *86*, 2939–2946.
- [29] N. N. Yazgan, İ. H. Boyacı, A. Topcu, U. Tamer, *Anal. Bioanal. Chem.* **2012**, *403*, 2009–2017.
- [30] H. Hu, Z. Wang, L. Pan, S. Zhao, S. Zhu, *J. Phys. Chem. C* **2010**, *114*, 7738–7742.
- [31] M. Gühlke, S. Selve, J. Kneipp, *J. Raman Spectrosc.* **2012**, *43*, 1204–1207.
- [32] J. Du, C. Jing, *J. Phys. Chem. C* **2011**, *115*, 17829–17835.
- [33] X. X. Han, A. M. Schmidt, G. Marten, A. Fischer, I. M. Weidinger, P. Hildebrandt, *ACS Nano* **2013**, *7*, 3212–3220.
- [34] J. Du, J. Cui, C. Jing, *Chem. Commun.* **2014**, *50*, 347–349.
- [35] B. Jun, M. S. Noh, J. Kim, G. Kim, H. Kang, M. Kim, Y. Seo, J. Baek, J. Kim, J. Park, *Small* **2010**, *6*, 119–125.
- [36] Q. Xu, *Ann. Phys.* **2012**, *524*, A161–A162.
- [37] L. Yang, P. Li, J. Liu, *RSC Adv.* **2014**, *4*, 49635–49646.
- [38] B. Han, N. Choi, K. H. Kim, D. W. Lim, J. Choo, *J. Phys. Chem. C* **2011**, *115*, 6290–6296.
- [39] Q. Gao, A. Zhao, Z. Gan, W. Tao, D. Li, M. Zhang, H. Guo, D. Wang, H. Sun, R. Mao, *CrystEngComm* **2012**, *14*, 4834–4842.
- [40] L. Yang, Z. Bao, Y. Wu, J. Liu, *J. Raman Spectrosc.* **2012**, *43*, 848–856.
- [41] Q. An, P. Zhang, J. Li, W. Ma, J. Guo, J. Hu, C. Wang, *Nanoscale* **2012**, *4*, 5210–5216.
- [42] T. Yang, X. Guo, H. Wang, S. Fu, J. Yu, Y. Wen, H. Yang, *Small* **2014**, *10*, 1325–1331.
- [43] Y. Ye, J. Chen, Q. Ding, D. Lin, R. Dong, L. Yang, J. Liu, *Nanoscale* **2013**, *5*, 5887–5895.
- [44] X. Hou, X. Zhang, S. Chen, H. Kang, W. Tan, *Colloids Surf. Physicochem. Eng. Aspects* **2012**, *403*, 148–154.
- [45] N. T. Trang, T. T. Thuy, K. Higashimine, D. M. Mott, S. Maenosono, *Plasmonics* **2013**, *8*, 1177–1184.
- [46] D. A. Wheeler, S. A. Adams, T. López-Luke, A. Torres-Castro, J. Z. Zhang, *Ann. Phys.* **2012**, *524*, 670–679.
- [47] D. Liu, X. Wang, D. He, T. D. Dao, T. Nagao, Q. Weng, D. Tang, X. Wang, W. Tian, D. Golberg, *Small* **2014**, *10*, 2564–2569.
- [48] Y. Wang, K. Wang, B. Zou, T. Gao, X. Zhang, Z. Du, S. Zhou, *J. Mater. Chem. C* **2013**, *1*, 2441–2447.
- [49] L. Zhang, W. Dong, Z. Tang, J. Song, H. Xia, H. Sun, *Opt. Lett.* **2010**, *35*, 3297–3299.
- [50] W. M. Carvalho, D. Volpati, V. A. Nunes Carvalho, R. F. Aroca, C. J. Constantino, F. L. Souza, *ChemPhysChem* **2013**, *14*, 1871–1876.
- [51] Z. Y. Bao, J. Dai, D. Y. Lei, Y. Wu, *J. Appl. Phys.* **2013**, *114*, 124305.
- [52] V. Amendola, M. Meneghetti, *Phys. Chem. Chem. Phys.* **2013**, *15*, 3027–3046.

- [53] V. Amendola, M. Meneghetti, O. M. Bakr, P. Riello, S. Polizzi, S. Fiameni, H. Dalaver, P. Arosio, T. Orlando, C. de Julian Fernandez, F. Pineider, C. Sangregorio, A. Lascialfari, *Nanoscale* **2013**, *5*, 5611–5619.
- [54] S. Scaramuzza, S. Agnoli, V. Amendola, *Phys. Chem. Chem. Phys.* **2015**, *17*, 28076–28087.
- [55] P. Wagener, J. Jakobi, C. Rehbock, V. S. Chakravadhanula, C. Thede, U. Wiedwald, M. Bartsch, L. Kienle, S. Barcikowski, *Sci. Rep.* **2016**, *6*, 23352.
- [56] Z. Swiatkowska-Warkocka, A. Pyatenko, F. Krok, B. R. Jany, M. Marszalek, *Sci. Rep.* **2015**, *5*, 9849.
- [57] G. C. Messina, M. G. Sinatra, V. Bonanni, R. Brescia, A. Alabastri, F. Pineider, G. Campo, C. Sangregorio, G. Li-Destri, G. Sfuncia, G. Marletta, M. Condorelli, R. Proietti Zaccaria, F. De Angelis, G. Compagnini, *J. Phys. Chem. C* **2016**, *120*, 12810–12818.
- [58] Z. Swiatkowska-Warkocka, K. Kawaguchi, Y. Shimizu, A. Pyatenko, H. Wang, N. Koshizaki, *Langmuir* **2012**, *28*, 4903–4907.
- [59] P. Boyer, D. Ménard, M. Meunier, *J. Phys. Chem. C* **2010**, *114*, 13497–13500.
- [60] X. Bao, M. Muhler, B. Pettinger, Y. Uchida, G. Lehmpfuhl, R. Schlögl, G. Ertl, *Catal. Lett.* **1995**, *32*, 171–183.
- [61] D. Badocco, I. Lavagnini, A. Mondin, P. Pastore, *Food Chem.* **2015**, *177*, 147–151.
- [62] I. Lavagnini, D. Badocco, P. Pastore, F. Magno, *Talanta* **2011**, *87*, 180–188.
- [63] F. Mafuné, J. Kohno, Y. Takeda, T. Kondow, H. Sawabe, *J. Phys. Chem. B.* **2000**, *104*, 9111–9117.
- [64] V. Amendola, M. Meneghetti, *Phys. Chem. Chem. Phys.* **2009**, *11*, 3805–3821.
- [65] P. Dutta, A. Manivannan, M. Seehra, N. Shah, G. Huffman, *Phys. Rev. B* **2004**, *70*, 174428.
- [66] F. Tournus, E. Bonet, *J. Magn. Magn. Mater.* **2011**, *323*, 1109–1117.
- [67] H. G. Fijolek, J. R. Grohal, J. L. Sample, M. J. Natan, *Inorg. Chem.* **1997**, *36*, 622–628.
- [68] I. G. Dance, K. J. Fisher, R. H. Banda, M. L. Scudder, *Inorg. Chem.* **1991**, *30*, 183–187.
- [69] H. J. Choi, S. W. Han, S. J. Lee, K. Kim, *J. Colloid Interface Sci.* **2003**, *264*, 458–466.
- [70] J. Horn, G. Onoda, *J. Am. Ceram. Soc.* **1978**, *61*, 523–527.
- [71] S. H. Behrens, D. G. Grier, *J. Chem. Phys.* **2001**, *115*, 6716–6721.
- [72] B. Liu, G. Han, Z. Zhang, R. Liu, C. Jiang, S. Wang, M. Han, *Anal. Chem.* **2012**, *84*, 255–261.
- [73] Q. Ye, J. Fang, L. Sun, *J. Phys. Chem. B* **1997**, *101*, 8221–8224.
- [74] T. Wang, X. Hu, S. Dong, *Small* **2008**, *4*, 781–786.
- [75] J. Liu, J. Wang, W. Huang, L. Yu, X. Ren, W. Wen, S. Yu, *Sci. Rep.* **2012**, *2*, 987.
- [76] T. Siegfried, M. Kind, A. Terfort, O. J. Martin, M. Zharnikov, N. Ballav, H. Sigg, *J. Raman Spectrosc.* **2013**, *44*, 170–175.
- [77] X. Li, G. Chen, L. Yang, Z. Jin, J. Liu, *Adv. Funct. Mater.* **2010**, *20*, 2815–2824.
- [78] Y. Zhou, J. Chen, L. Zhang, L. Yang, *Eur. J. Inorg. Chem.* **2012**, *2012*, 3176–3182.
- [79] G. Sinha, L. E. Depero, I. Alessandri, *ACS Appl. Mater. Interfaces* **2011**, *3*, 2557–2563.
- [80] S. Xu, Y. Zhang, Y. Luo, S. Wang, H. Ding, J. Xu, G. Li, *Analyst* **2013**, *138*, 4519–4525.
- [81] J. Liu, R. H. Hurt, *Environ. Sci. Technol.* **2010**, *44*, 2169–2175.

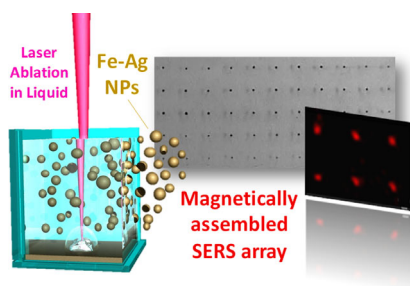
Manuscript received: June 16, 2016
Accepted Article published: August 23, 2016
Final Article published: ■ ■ ■, 2016

ARTICLES

S. Scaramuzza, D. Badocco, P. Pastore,
D. F. Coral, M. B. Fernández van Raap,
V. Amendola*



Magnetically Assembled SERS Substrates Composed of Iron–Silver Nanoparticles Obtained by Laser Ablation in Liquid



Joining forces: Bimetallic iron–silver nanoparticles (NPs) can be synthesized by laser ablation, with surface-enhanced Raman spectroscopy (SERS) performances, ready responses to magnetic fields, and complete flexibility in surface coating, and used for the magnetic assembly of SERS substrates. Magnetic assembly allows a significant increase in the SERS signal of analytes compared with non-assembled NPs (see figure).